

Distribution of density along magnetospheric field lines

R. E. Denton,¹ K. Takahashi,² I. A. Galkin,³ P. A. Nsumei,³ X. Huang,³ B. W. Reinisch,³
R. R. Anderson,⁴ M. K. Sleeper,¹ and W. J. Hughes⁵

Received 8 September 2005; revised 7 December 2005; accepted 10 January 2006; published 21 April 2006.

[1] This paper examines the field line distribution of magnetospheric electron density and mass density. The electron density distributions from IMAGE RPI active sounding are generally monotonic. The density increases with increasing MLAT slightly faster than the dependence found from the field line dependence model of Denton et al. (2002b); in general, a power law dependence $n_e = n_{e0} (LR_E/R)^\alpha$ with $\alpha \sim 1$ appears to be appropriate within the plasmasphere, at least for geocentric radius $R > 2 R_E$. Our comparison to RPI data included also one field line distribution at $L_T = 7.4$, which we fit with $\alpha = 2.5$, a value typical of the plasmatrough based on previous studies. We calculated the average electron density field line distribution at low MLAT using the CRRES plasma wave data and found that the density was relatively flat near the magnetic equator with no convincing evidence for an equatorial peak. Using the average values of toroidal Alfvén frequencies, we calculated the mass density field line distributions and found that they were roughly monotonic for $L_T < 6$, with $\alpha = 2$ appropriate for $L_T = 4-5$ and $\alpha = 1$ appropriate for $L_T = 5-6$. At $L_T = 6-8$, the distribution was nonmonotonic, with a local peak in mass density at the magnetic equator. Dividing the frequency data into different groups based on activity, we found that the inferred average mass density field line dependence was insensitive to geomagnetic activity at $L_T = 4-6$ but that at $L_T = 6-8$, the tendency for the mass density to be peaked at the magnetic equator increased with respect to larger Alfvén wave amplitude and more negative Dst. The average frequency ratios at $L_T = 6-8$ did not change if we limited the data to cases with MLT = 8–16, for which the assumed perfect conductor boundary condition was better justified. Taken together, these results imply that heavy ions are preferentially peaked at the magnetic equator for $L_T = 6-8$, at least during more geomagnetically active periods.

Citation: Denton, R. E., K. Takahashi, I. A. Galkin, P. A. Nsumei, X. Huang, B. W. Reinisch, R. R. Anderson, M. K. Sleeper, and W. J. Hughes (2006), Distribution of density along magnetospheric field lines, *J. Geophys. Res.*, *111*, A04213, doi:10.1029/2005JA011414.

1. Introduction

[2] Magnetospheric density controls the rate of response of the magnetosphere to perturbations. Mass density controls the rate of response to low-frequency perturbations for which the ions oscillate (ULF waves), while electron density controls the rate of response to high-frequency perturbations for which only the electrons respond (VLF and radio waves). Recent research has shown that magnetospheric waves have an important effect on particle populations. Radiation belt electrons may be energized by

global scale Alfvén waves or whistler chorus and may be scattered into the loss cone by whistler chorus or electromagnetic ion cyclotron (EMIC) waves [Elkington et al., 2003; Meredith et al., 2003; Summers et al., 2004; Perry et al., 2005]. Ring current protons may also be lost due to EMIC waves [Spasojevic et al., 2004]. In order to understand the growth and propagation of these waves and to understand their effect on particle populations, it is necessary to understand the distribution of density along magnetic field lines.

[3] Several recent studies have yielded information about the field line distribution of magnetospheric density. Goldstein et al. [2001], and Denton et al. [2002a, 2002b, 2004a, 2004b] studied the average distribution of electron density along magnetic field lines using local electron density measurements based on data from the Polar spacecraft Plasma Wave Instrument (PWI). Except for the study by Denton et al. [2002a], all these investigations used the power law form to describe the field line distribution,

$$n_e = n_{e0} (L_T R_E / R)^\alpha, \quad (1)$$

¹Department of Physics and Astronomy, Dartmouth College, Hanover, New Hampshire, USA.

²Johns Hopkins University Applied Physics Laboratory, Laurel, Maryland, USA.

³Center for Atmospheric Research, University of Massachusetts at Lowell, Lowell, Massachusetts, USA.

⁴Department of Physics and Astronomy, University of Iowa, Iowa City, Iowa, USA.

⁵Department of Astronomy, Boston University, Boston, Massachusetts, USA.

where $L_T R_E$ is the maximum geocentric radius R to any point on the field line based on a Tsyganenko magnetic field model ($= LR_E$ for a dipole field), and n_{e0} is the value of n_e where $R = L_T R_E$. The magnetic field model used in these studies and also in this paper is the T96 model [Tsyganenko, 1995] if solar wind data are available or the T89 model [Tsyganenko, 1989] otherwise. The maximum radius $R = L_T R_E$ occurred at the position of minimum magnetic field B_0 , which we call the magnetic equator. (Data points for which this was not true were excluded from the studies.) Note that $\alpha = 0$ in (1) implies that n_e is constant along field lines and that increasingly positive values of α lead to steeper increase in n_e with respect to increasing magnetic latitude MLAT (i.e., decreasing R). (Increasing MLAT corresponds to smaller R .) A general result from all of these studies was that the density dependence was relatively flat ($\alpha \sim 0-1$) in the high-density plasmasphere at small L_T , whereas the density was steeper ($\alpha \sim 2-3$) in the low-density plasmatrrough at larger L_T . As discussed by Takahashi *et al.* [2004], $\alpha = 0-1$ is roughly consistent with diffusive equilibrium solutions, at least for $R \gtrsim 2R_E$ sampled by the Polar data. The value $\alpha = 2$ is intermediate between the dependence expected for diffusive equilibrium and so called collisionless models, for which $\alpha \sim 3$ or 4 [see also Lemaire and Gringauz, 1998]. Denton *et al.* [2002b] modeled the average of α as a function of the equatorial density n_{e0} and L_T for both plasmasphere and plasmatrrough data,

$$\begin{aligned}\alpha_{\text{model}} &= \alpha_{n_{e0}} + \alpha_{L_T} \\ \alpha_{n_{e0}} &= 6.0 - 3.0 \log_{10} n_{e0} + 0.28(\log_{10} n_{e0})^2, \\ \alpha_{L_T} &= 2.0 - 0.43L_T,\end{aligned}\quad (2)$$

with an average error in α of 0.65. Denton *et al.* [2004b] showed that there was no remaining dependence of the average α on MLT or Kp.

[4] Recently, the field line dependence of electron density has been investigated using the Radio Plasma Imager (RPI) instrument on the IMAGE spacecraft [Reinisch *et al.*, 2001, 2004; Huang *et al.*, 2004]. The radio signals that are emitted by RPI then reflect where the wave frequency is equal to the local plasma frequency and then are subsequently detected by RPI, are apparently ducted along field lines [Reinisch *et al.*, 2001]. The RPI field line dependence has been described using

$$n_e = n_{e0}(\cos((\pi/2)\lambda/(0.8\lambda_{\text{inv}})))^{-\beta}, \quad (3)$$

where λ_{inv} is the invariant (Earth's surface) value of the latitude λ ($=$ MLAT) [Reinisch *et al.*, 2004; Huang *et al.*, 2004]. This equation is similar to $n_e = n_{e0}(\cos(\lambda))^{-2\alpha}$, which follows from (1) for a dipole magnetic field. So far, published density profiles for closed field lines have been for relatively low L shell within the plasmasphere. (Other studies have looked at the density dependence in the polar cap [Nsumei *et al.*, 2003].) No systematic attempt has been made to relate the RPI data to (1), but Denton *et al.* [2002a] presented an argument that in the vicinity of the magnetic equator, the RPI data were roughly consistent with a low-value $\alpha \sim 3/4$. (At higher latitudes, the field

line dependence may diverge significantly from this dependence.)

[5] Direct measurement of the field line dependence of ion species is difficult, owing to the difficulty in measuring cold ions and the strong dependence of density across field lines; nevertheless, Gallagher *et al.* [2000] found that the sum of the H⁺ and He⁺ densities was roughly constant along field lines within the plasmasphere in the range $L_T R_E = 3-5R_E$ for $R > 2R_E$.

[6] The field line dependence of mass density has also been investigated using the frequencies of toroidal Alfvén waves. Because the harmonics of these waves have different field line structure, they respond differently to mass density at various locations along the field line. For instance, the fundamental mode, with an antinode in the electric field perturbation (radial) and velocity perturbation (azimuthal) at the equator, is slowed down by a concentration of mass density at the magnetic equator, while the second harmonic, with a node for these quantities at the magnetic equator, is not. Thus the ratios of the harmonic frequencies can be used to infer the field line distribution of mass density. Takahashi *et al.* [2004] used an automated technique to determine the frequencies of toroidal Alfvén wave harmonics observed by the CRRES spacecraft and from the average frequency ratios found that the inferred mass density was relatively flat for low $L_T \lesssim 6$ with $\alpha \sim 0-1$. This result is consistent with the field line dependence of electron density based on the statistical studies using Polar PWI and is roughly consistent with diffusive equilibrium along the field line [Takahashi *et al.*, 2004]. At larger values of L_T , the values of the average frequency ratios indicated that the mass density was locally peaked at the magnetic equator. The inferred mass density field line distribution decreased from its value at the magnetic equator to a value about a factor of two lower at MLAT = 17° and then increased at larger MLAT (though the uncertainty in the inferred distribution at large MLAT was very large). This result was also consistent with a detailed study of two events [Denton *et al.*, 2004a].

[7] Thus while the studies of electron density, ion density, and mass density have all indicated a relatively flat field line dependence for the plasmasphere ($\alpha \sim 0-1$), there is some disagreement about the field line distribution at large L_T (within the plasmatrrough, or extended plasmasphere [Denton *et al.*, 2004b]). The purpose of this investigation is to reexamine the field line dependence of both electron density and mass density. In the case of electron density, we use different data sets (CRRES and IMAGE RPI). For the mass density, we make some improvements in technique and show new results. It should be emphasized at the outset, however, that the results published to date are not necessarily contradictory. There may be a concentration of heavy ions at the magnetic equator due the centrifugal force (due to rotation), which can lead to an effective gravitational potential well at the magnetic equator. Lemaire and Gringauz [1998] discussed such a potential well in the context of a critical L value, $L_c = 5.78$, beyond which the effect becomes important. Note that $L_c = 5.78$ is nearly equivalent to $L_T = 6$, beyond which Takahashi *et al.* [2004] found mass density to be locally peaked at the magnetic equator. If the temperatures of multiple ion species are similar, the centrifugal force would more effectively trap heavy ions (e.g., O⁺) at the equator than light ones, which could result in a concen-

Table 1. RPI Fit-Model Comparison

Item	Reference			
	<i>Reinisch et al.</i> [2001, Figure 3]	<i>Huang et al.</i> [2004, Figure 3]	<i>Reinisch et al.</i> [2004, Figure 1]	<i>Reinisch et al.</i> [2004, Figure 5]
Date	24 Oct 2000	8 Jun 2001	30 Mar 2001	1 Apr 2001
UT	1750	2037	2116	1608
Plotted here in	Figure 1a	Figure 1b	Figure 1c	Figure 1d
L	3.0	3.23	3.32	2.84
MLT	22.8	8.0	12.2	12.2
Kp	1.4	2.3	3.2	3.0
$\langle Kp \rangle_3$	2.12	1.79	3.09	4.79
$n_{e0-fit}, \text{cm}^{-3}$	849.	777.	537.	428.
$n_{e0-model}, \text{cm}^{-3}$	853.	783.	547.	439.
α_{fit}	1.1	0.8	0.8	2.3
α_{model}	0.3	0.3	0.5	0.8
$\alpha_{fit} - \alpha_{model}$	0.8	0.5	0.3	1.5

tration of mass density but not electron density at the magnetic equator (K. Ferriere, private communication, 2005).

[8] In section 2, we examine new results for the field line dependence of electron density. This includes a comparison of IMAGE RPI data to the predictions of our field line dependence model (section 2.1), and a statistical study of the MLAT dependence near the magnetic equator using CRRES data (section 2.3). In section 3, we reexamine the field line dependence of mass density based on toroidal Alfvén waves observed by the CRRES spacecraft. Using the database of harmonic frequencies determined by *Takahashi et al.* [2004], we examine the field line dependence for various L_T ranges in section 3.1 and consider the variation in field line dependence due to different values of Dst, Kp, and wave amplitude in section 3.2. A summary of results is given for electron density in section 2.4 and for mass density in section 3.3. Finally, we present our conclusions in section 4.

2. Electron Density

2.1. Comparison With n_e Profiles Determined From IMAGE RPI

[9] Using radio sounding, the RPI (Radio Plasma Imager) instrument on the IMAGE spacecraft has measured the field line distribution of electron density in several cases [*Reinisch et al.*, 2001, 2004; *Huang et al.*, 2004]. Values of n_e versus MLAT were determined for four different RPI observations by digitizing the data from the figures listed in Table 1.

[10] The field line distributions of the RPI density are plotted in Figure 1 (thick solid curves) for the four events. The time periods corresponding to Figure 1a and Figure 1b are relatively quiet, as indicated by the low Kp or $\langle Kp \rangle_3$ values in Table 1 (Kp = 1.4 and 2.3, respectively, or $\langle Kp \rangle_3 = 2.1$ and 1.8, respectively). The observations shown in Figures 1c and 1d occur during a more active period ($\langle Kp \rangle_3 = 3.1$ and 4.8, respectively) just before and just after a major magnetic storm (hourly Dst = -380), in which there was a major depletion of density [*Reinisch et al.*, 2004].

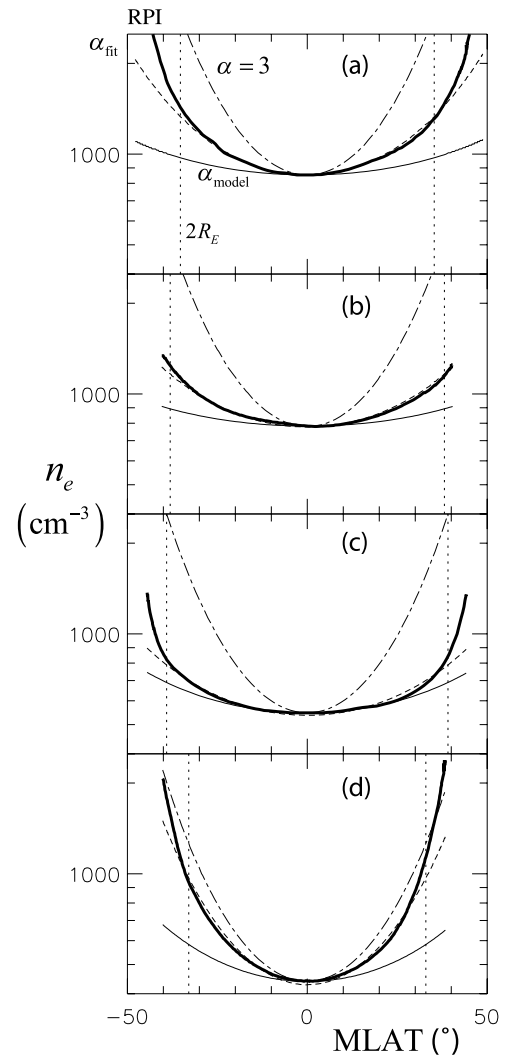


Figure 1. Field line distribution of n_e versus MLAT measured by the RPI instrument (thick solid curve) and the power law distribution using α_{model} (equation (2)) (thin solid curve) for the events listed in Table 1. The dashed curve is the power law distribution that best fits the RPI data between the magnetic equator and $R = 2 R_E$ (vertical dotted lines), while the dot-dashed curve is the power law distribution with $\alpha = 3$. The times and references for the four events (a–d) are listed in Table 1.

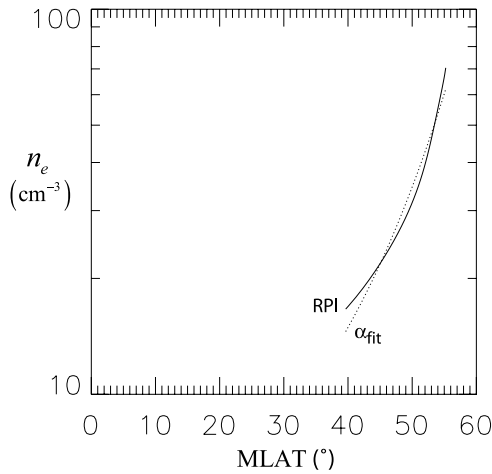


Figure 2. Field line distribution of n_e versus MLAT measured by the RPI instrument (solid curve) and the power law distribution that best fits the RPI data (dotted curve) from active sounding by IMAGE RPI at 2 June 2001, 0729 UT. Here $L_T = 7.4$.

[11] The vertical dotted lines in Figure 1 are plotted at a MLAT value corresponding to geocentric radius $R = 2 R_E$. The dashed curves in Figure 1 represent the power law distribution of n_e that best fits the RPI data for $R \geq 2 R_E$ (between the vertical dotted lines). The power law fit parameters, $n_{e0-\text{fit}}$ and α_{fit} , are listed for each event in Table 1. The good match between the dashed curves and the thick solid curves in Figure 1 indicates that the power law functional form (equation (1)) is capable of representing the RPI distribution for these R values. The electron density based on α_{model} (equation (2)) (developed for $R \geq 2R_E$) is plotted as the thin solid curves in Figure 1. The power law parameters for the model, $n_{e0-\text{model}}$ and α_{model} , are also listed in Table 1. The value of $n_{e0-\text{model}}$ is the n_e value measured by RPI at MLAT = 0. The final item listed in Table 1 is the difference $\alpha_{\text{fit}} - \alpha_{\text{model}}$, which gives a good estimate of how well the model fits the RPI data. While two of the values of $\alpha_{\text{fit}} - \alpha_{\text{model}}$ are within the uncertainty of the model (0.65; see section 1), two are not. Furthermore, there seems to be a trend that RPI finds a steeper increase in density with respect to MLAT than that implied by α_{model} (equation (2)). If future analysis shows that the field line dependence observed by IMAGE RPI is consistently steeper than the average dependence inferred from the Polar data, it could possibly be due to a bias in the Polar data to exclude the largest equatorial densities at $L_T \lesssim 3$ due to the preamplifier oscillation problem mentioned by *Goldstein et al.* [2001] and *Denton et al.* [2002a]. Despite this possible problem, the first three of the cases listed in Table 1 have α_{fit} values that are within or very close to the $\alpha = 0-1$ range we have suggested for the field line dependence of plasmaspheric electron density [*Denton et al.*, 2004b].

[12] The fourth density profile (*Reinisch et al.* [2004, Figure 5], Table 1, and Figure 1d) is significantly steeper with respect to MLAT than our model predicts, with $\alpha_{\text{fit}} = 2.3$. This observation at $L = 2.84$ occurred during a geomagnetic storm, and the plasmopause had moved in to a very low value of $L = 2.2$ *Reinisch et al.* [2004]. The

resulting α value (2.3), is typical for the plasmatrough [*Goldstein et al.*, 2001; *Denton et al.*, 2002a, 2002b, 2004b], though $L = 2.84$ is usually within the plasmasphere. Aside from this last case, it looks like $\alpha \sim 1$ is appropriate for describing the electron density distribution at $L_T \sim 3$, at least for $R \gtrsim 2R_E$.

[13] Up until now, the published profiles of n_e from RPI active sounding have been for low L values. However, using the same method as *Reinisch et al.* [2001], we have determined the field line distribution of electron density for $L_T = 7.4$ at 2 June 2001, 0729 UT. At this time, the RPI instrument was emitting coded signals at frequencies between 0.3 and 615 kHz and reflected echoes were detected with delay time depending on the frequency. Active sounding echoes were obtained only from the direction down the field line toward the northern polar region. On the basis of previous results when several echo traces were measured [*Reinisch et al.*, 2001], we assumed that the reflected echoes propagated in the X-mode along the magnetic field line. Then, using the cold plasma dispersion relation and the T96 magnetic field model [*Tsyganenko*, 1995], the group velocity along the field line can be found as a function of n_e , and this can be used to relate the echo delay time to distance along the field line. The electron density profile inferred from the RPI active sounding is shown as the solid curve in Figure 2, while the best fit curve using the power law distribution with $\alpha_{\text{fit}} = 2.5$ (and $n_{e0} = 3.29$) is shown as the dotted curve. This value of $\alpha = 2.5$ is consistent with previous results from Polar data in the plasmatrough [*Denton et al.*, 2004b]. Using $n_{e0} = 3.29$ and $L_T = 7.43$, we find from (2) $\alpha_{\text{model}} = 3.3$.

[14] As was indicated in section 1, results for the field line dependence of mass density had indicated that the mass density is locally peaked within 10 to 30° of the magnetic equator for large $L_T \gtrsim 6$ [*Denton et al.*, 2004a; *Takahashi et al.*, 2004]. Note that the RPI active sounding cannot give us the electron density at lower latitudes than the spacecraft position. (The waves that would reflect at the low latitudes are at too low a frequency to propagate through the plasma at the spacecraft position. The most we could hope to get for Figure 2 is the profile of density at high latitude in the Southern Hemisphere as well as in the Northern Hemisphere, but this was not observed.) Since IMAGE was at MLAT = 39.6°, the RPI active sounding data at 2 June 2001, 0729 UT (Figure 2) cannot give us information about whether or not the electron density is locally peaked at the magnetic equator.

2.2. MLAT Dependence of Polar Data

[15] Our assumed form for the field line dependence of the electron density (1) based on the Polar PWI data is monotonic with respect to MLAT and therefore also does not include a local peak at the magnetic equator. However, the Polar data from which (2) was inferred also did not sample low values of MLAT when L_T was large. To illustrate this fact, we plot in Figures 3 and 4 the log average electron density binned with respect to MLAT for the plasmasphere and plasmatrough, respectively. As described by *Denton et al.* [2002b], the division between plasmasphere and plasmatrough data was determined by visual inspection. A plasmopause (dividing the two regions) was identified if there was a drop in n_e of at least a factor of

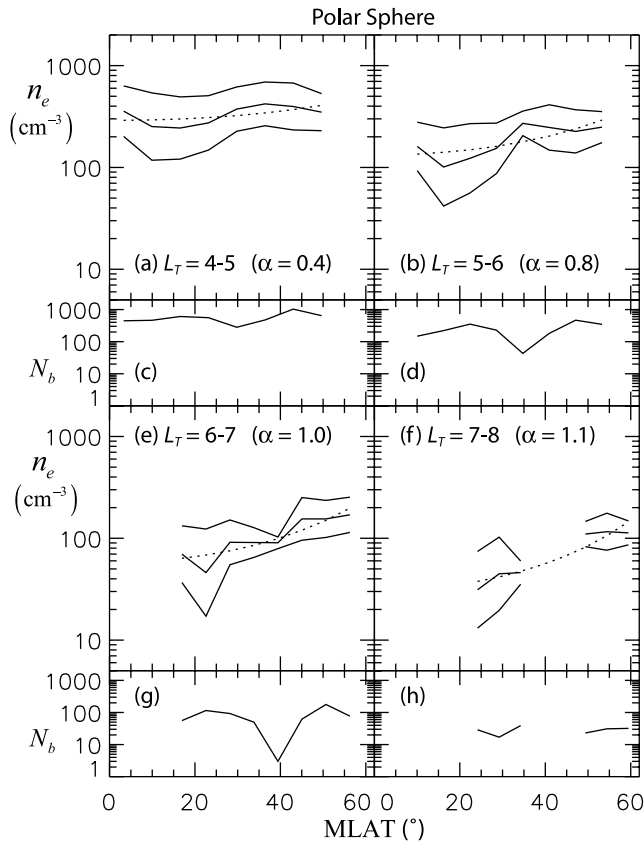


Figure 3. On the basis of the Polar PWI plasmasphere data set of *Denton et al.* [2002a], (a) the log average electron density (middle solid curve), the log average plus or minus one standard deviation (upper and lower solid curves), and the best power law fit (dashed curve), and (c) the number of data points within each MLAT bin N_b with respect to MLAT for $L_T = 4-5$. (b) and (d) $L_T = 5-6$, (e) and (g) $L_T = 6-7$, and (f) and (h) $L_T = 7-8$. The power law coefficient used for the corresponding dashed curves Figures 3a, 3b, 3e, and 3f is listed in each of these panels.

three within $\Delta L_T = 0.4$. The plasmasphere data set includes data with no plasmopause (Denton et al.’s “gradually decreasing category”), which may extend out (at least under quiet conditions) to large L_T as described by *Denton et al.* [2004b]. (For more details, see *Denton et al.* [2002b] or *Denton et al.* [2004b, Appendix A].)

[16] In Figures 3 and 4, panels a, b, e, and f show the log average value of n_e (middle solid curve), the log average plus or minus one standard deviation (upper and lower solid curves), and the best power law fit to the data (dashed curves) for $L_T = 4-5$, $5-6$, $6-7$, and $7-8$, respectively. These plots, and all the remaining plots of density versus latitude in this paper, show the density versus the absolute value of the latitude; it is assumed that the density is symmetric with respect to the magnetic equator. (Only in Figure 1 was there a possibility of asymmetry in the n_e values inferred from active radio sounding.) Below each of these panels, in panels c, d, g, and h, are the number of data points (corresponding to pairs of Polar PWI measurements at different radius) for the corresponding ranges of L_T . Listed in the panels showing n_e (panels a, b, e, and f) next to

the L_T range are the α values for the best fit to the data (dashed curves). (As is clear from Figures 3 and 4, these values generally characterize the large-scale MLAT variation from MLAT $\sim 20^\circ$ to MLAT $\sim 50^\circ$.) These α values are generally consistent with conclusions we have previously published [e.g., *Denton et al.*, 2004b] that $\alpha = 0-1$ is typical for the plasmasphere, while $\alpha = 2-3$ is typical for the plasmatrough.

[17] However, note that at large $L_T > 6$, low values of MLAT $< 20^\circ$ were not sampled. (This was not obvious based on the plots of n_e versus geocentric radius R in the work of *Denton et al.* [2002a] because the $0-20^\circ$ range in MLAT maps to only a small change in R .) Thus the Polar PWI data are not a good indicator of whether or not there is a local peak in electron density at the magnetic equator at $L_T > 6$.

2.3. Statistical Distribution at Low MLAT Based on Data From CRRES

[18] To investigate whether or not there is a peak in electron density at the magnetic equator for $L_T > 6$, we examined the CRRES Plasma Wave Experiment (PWE) data. CRRES, with its low-altitude (18° inclination) geosynchronous transfer orbit, did sample the region around MLAT = 0° . The electron density in the CRRES database was found either from the narrow band emission at the upper hybrid frequency or from the cutoff in continuum radiation at the plasma frequency [*LeDocq et al.*, 1994]. Data were collected between 1 August 1990 and 12 October

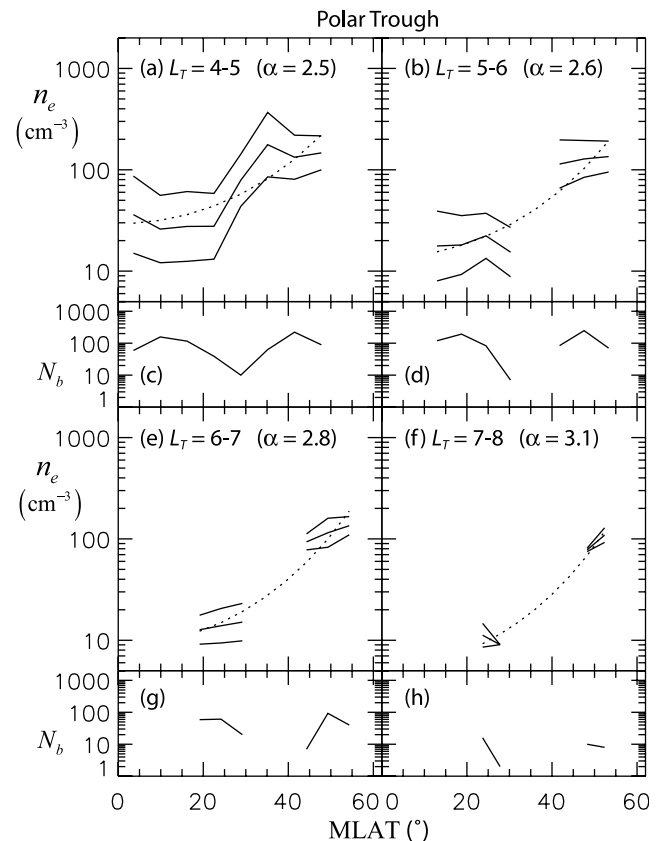


Figure 4. Same as Figure 3, but using the plasmatrough data set of *Denton et al.* [2002a].

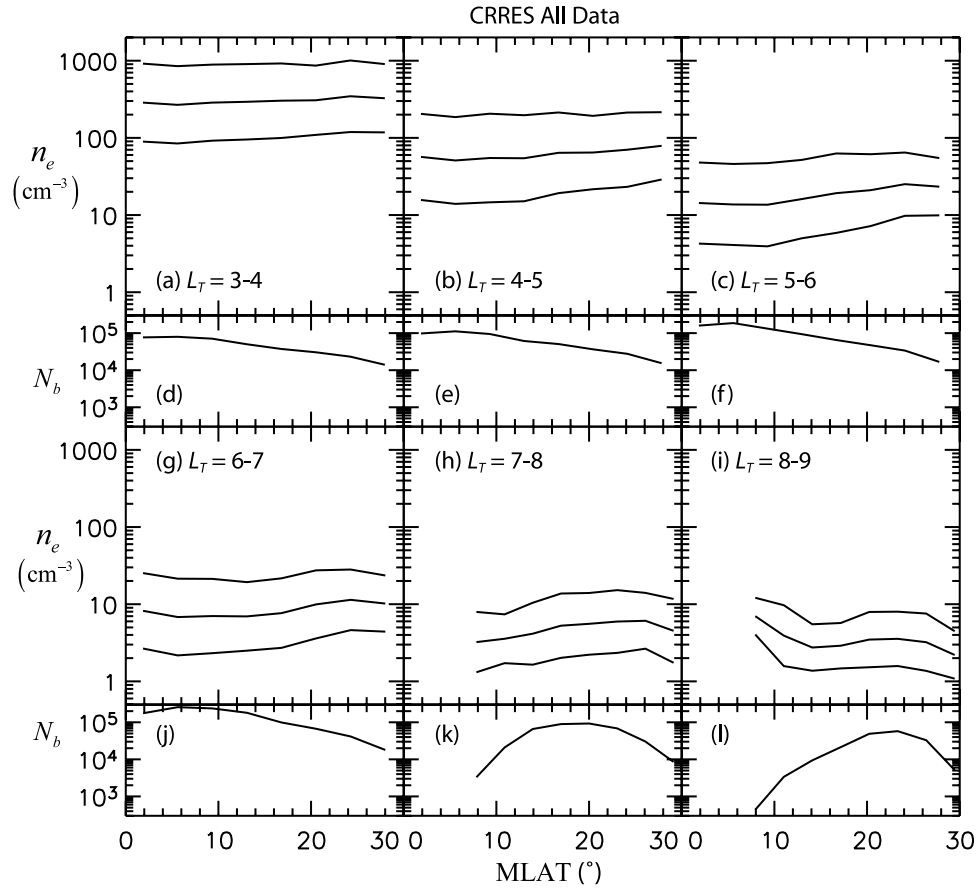


Figure 5. Based on the CRRES PWE n_e data, (a) the log average electron density (middle solid curve), and the log average plus or minus one standard deviation (upper and lower solid curves), and (d) the number of data points per MLAT bin N_b , as a function of MLAT for $L_T = 3-4$. The other panels show the same data for the L_T ranges listed in the panels plotting n_e .

1991. Altogether there are 334 days of data at 8 s resolution in time. The local time coverage included all values except MLT = 9–12. From the beginning of this time period to about 1 June 1991, the average Kp value was about 2. From 1 June on (with CRRES sampling MLT = 12–21), the activity was higher; there were a number of geomagnetic storms and the average Kp was about 4.

[19] Figure 5 shows the CRRES data binned versus MLAT for the L_T ranges indicated in the figure. (The binned MLAT values are the absolute value of MLAT - MLAT_{Rmax}, where MLAT_{Rmax} is the MLAT value at the point on the field line where the radius $R = R_{\text{max}} = L_T R_E$ is a maximum. The value MLAT = MLAT_{Rmax} is a better indicator of MLAT at the real magnetic equator than is MLAT = 0.) In the plots of n_e (panel a for $L_T = 3-4$), the middle curve is the log average value, and the upper and lower curves are the log average plus or minus one standard deviation. Below the panels with n_e are plots of the number of data points per MLAT bin N_b (Figure 5d for $L_T = 3-4$). Figure 5 shows that there is no clear indication from the CRRES data of a local peak in n_e for L_T up to 7. At $L_T = 6-7$, there may be a slight peak in n_e near MLAT = 0°, but the difference between the local minimum density and equatorial density is definitely less than the factor of two increase over a broad angular range

(between MLAT = 0 and 20°) inferred for the mass density from Alfvén frequency ratios (see section 3.1). At $L_T = 7-8$, there is no indication of a local peak in n_e outside of MLAT = 8°. At $L_T = 8-9$, there could be evidence of a peak in n_e based on the binned values of n_e between MLAT = 8 and 14°. Note, however, that the statistics are not nearly as good for the lowest MLAT bin at $L_T = 8-9$ as for the other bins (as indicated by the relatively low value of N_b ; the CRRES data time resolution is 8 s so that $N_b \sim 500$ represents about an hour of data) and that the magnetic field models are not as reliable at such large values of L_T as 8–9.

[20] Figure 6 is the same as Figure 5 except that the data have been limited to cases for which $n_{e0} < (15 \text{ cm}^{-3})(6.6/L_T)^4$. This limit was used by Denton *et al.* [2004b] (motivated by the study of Sheeley *et al.* [2001]) to roughly approximate the plasmatrough data set. (For the purposes of evaluating this limit only, (2) was used to get n_{e0} from n_e . The data were then binned versus MLAT using n_e .) Figure 6 does not show any clear evidence for a local peak in n_e at the magnetic equator.

2.4. Summary of Electron Density Observations

[21] On the basis of the Polar PWI data, a model for the average α was developed (equation (2)), which with (1) can be used to model the field line dependence of electron

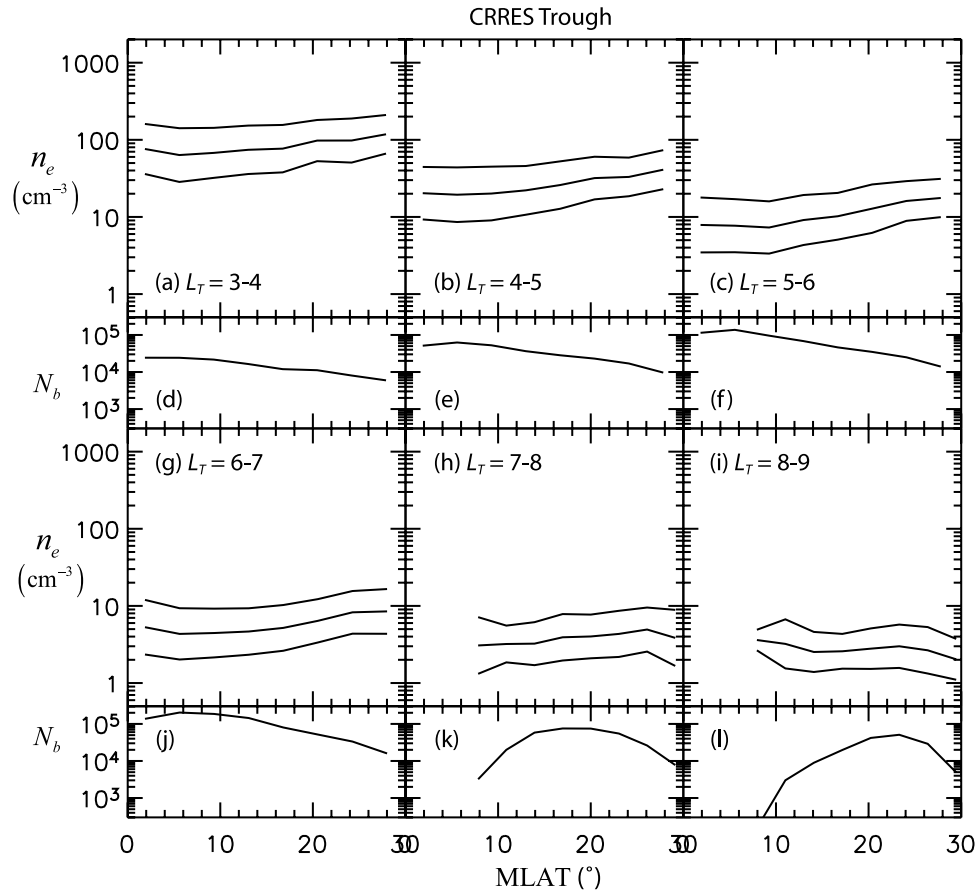


Figure 6. Same as Figure 5, except that the CRRES data were limited to those cases with $n_{e0} < (15 \text{ cm}^{-3})(6.6/L_T)^4$, thereby approximating a plasmatrough data set.

density [Denton *et al.*, 2002b]. Using IMAGE RPI active sounding data, we tested this model. The α values for a best power law fit to the RPI data are generally close to, but somewhat higher than the model values. On the basis of the RPI data combined with the Polar data shown in section 2.2, it appears that $\alpha \sim 1$ is usually appropriate within the plasmasphere, at least for $R > 2R_E$. However, during a severe storm, the equatorial density may be depleted even at low L [Reinisch *et al.*, 2004] so that the field line dependence is steeper there ($\alpha = 2.3$ for the case shown in section 2.1, a value typical for the plasmatrough). Our comparison to RPI data included one case at $L_T > 6$. However, the observed electron density for this case, and also the Polar PWI data on which (2) was based (Figures 3 and 4), are limited to large MLAT $> 20^\circ$. In order to see if there was any evidence for a local peak in electron density near the magnetic equator, we also examined electron densities from the CRRES plasma wave data. There appears to be no convincing evidence from this data set for such a local peak (Figures 5 and 6). There may be a small peak at $L_T = 6-7$, but if so, the ratio of the equatorial density to the local minimum density is lower than that for the mass density inferred from Alfvén frequency ratios (see section 3.1), and the peaking occurs over a narrower angular range. There is stronger evidence for local peaking of n_e at the magnetic equator for $L_T = 8-9$, but in this L_T range the MLAT coverage is not complete, the magnetic field model

is not reliable, and the statistical error is larger than for the other L_T ranges.

3. Field Line Distribution of Mass Density

[22] Taken together, the evidence for a local peak in mass density at the magnetic equator [Takahashi *et al.*, 2004; Denton *et al.*, 2004a] and the lack of evidence for such a peak in electron density (at least for $L_T < 8$; see section 2.3) indicate that heavy ions are preferentially concentrated at the magnetic equator. We now reexamine the CRRES toroidal Alfvén frequency data, in order to see if we can get a better idea of what could cause peaking of the mass density.

3.1. Field Line Distribution From Frequencies of Takahashi *et al.* [2004]: Variation With L_T

[23] Takahashi *et al.* [2004] used an automated technique to detect toroidal Alfvén frequencies in the CRRES magnetic and electric field data. From these frequencies, the fundamental frequency was selected, and all the observed frequencies were normalized to the nearby values of the fundamental frequency. Here, we redo the analysis with several modifications. The most important modification is that we bin the frequency ratios by L_T rather than the dipole L shell. A second major modification is that we screen out data points for which the uncertainty in a harmonic frequency (from the automated procedure) is greater than the

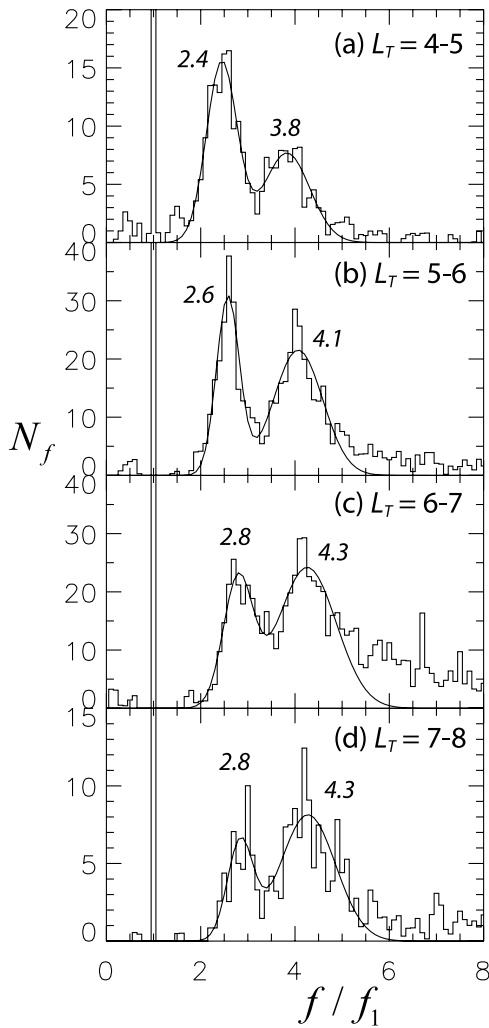


Figure 7. Histogram of the ratio of the toroidal Alfvén harmonic frequency f divided by the fundamental frequency f_1 for different ranges of L_T . N_f is the number of wave observations in each bin of width 0.1. The curves in each panel are a superposition of two Gaussians with parameters adjusted to minimize the standard error.

frequency of the fundamental. We also expand the data set to include measurements at all local times. (Takahashi *et al.* [2004] limited their analysis to the toroidal Alfvén frequencies observed in the afternoon local time sector, MLT = 12–18. This is not a major modification, since only 11% of the new data set is outside of MLT = 12–18.) We also use a slightly different binning procedure that is less noisy (linear interpolation for binning rather than nearest neighbor). Finally, we limited the analysis to the electric field data, which are higher quality than the magnetic field data due to noise from incorrect despinning of the magnetic field data. (See Takahashi *et al.* [2004] for more details concerning the analysis.)

[24] Histograms of our frequencies normalized to the fundamental frequency f/f_1 are shown in Figure 7. Gaussian peaks for the second and third Alfvén wave harmonics were automatically fit to the histograms, and the peak ratios for f_2/f_1 and f_3/f_1 are displayed above these peaks. Comparison

of Figure 7 with Figure 8 of Takahashi *et al.* [2004], shows that the new results are similar except for the $L_T = 7-8$ range, for which our figure (Figure 7d) has much better defined harmonic peaks. (In this largest range of L_T , the difference between the Tsyganenko and dipole magnetic field models is the greatest.)

[25] The frequency ratios based on the data shown in Figure 7 are listed in Table 2. We now use these ratios to calculate the field line distribution of mass density. The procedure is the same as that used by Takahashi *et al.* [2004] and Denton *et al.* [2004b]. The Singer *et al.* [1981] wave equation, based on MHD, is solved for the wave frequencies. This equation can be used for an arbitrary magnetic field, but the wave equation is strictly valid only for azimuthal oscillations (toroidal Alfvén wave) within an azimuthally symmetric equilibrium. Here, for the solution of the wave equation, we use a dipole field, since Takahashi *et al.* [2004] did not find much difference in the field line distribution versus MLAT if a Tsyganenko magnetic field model was used, and to use such a model, we have to make assumptions about time, position, and the solar wind parameters. A perfect conductor boundary condition is assumed at a height of 500 km above the Earth’s surface. (A lower height ~ 100 km would have been better [Denton *et al.*, 2006], but at these values of L_T , there is very little difference in the resulting field line distribution except near the Earth.) The assumed form for the mass density field line distribution is a polynomial with respect to the Alfvén crossing time coordinate, $\tau = \int ds/V_A$, where s is the distance along the field line from the magnetic equator toward the North Pole and V_A is the Alfvén speed. (This is the logical coordinate to use since within the WKB approximation, the wave functions will be sinusoidal with respect to this coordinate.) The procedure for calculating the distribution of mass density is to make an initial guess for the polynomial coefficients and then adjust the coefficients so as to minimize the difference between the observed frequencies and the theoretical ones.

[26] We assume that the mass density is symmetric with respect to the magnetic equator. Since we only have two frequency ratios, the polynomial can only include three terms, a constant term, and terms proportional to τ^2 and τ^4 . (In addition to the two frequency ratios, there is a constraint that the standard error between the theoretical and observed frequencies is minimized.) The resulting density distribution can be monotonic with respect to MLAT or there can be a local maximum or minimum at the magnetic equator.

[27] Figure 8 shows the inferred field line distributions of mass density ρ versus MLAT for $L_T=4-5$ (Figure 8a), $L_T=5-6$ (Figure 8b), $L_T=6-7$ (Figure 8c), and $L_T=7-8$ (Figure 8d). (The fundamental frequency is chosen so that the solution based on the peak frequency ratios has $\rho = 1$ at MLAT = 0; therefore only the relative variation in ρ within each panel of Figure 8 is significant.) The bold curves are the

Table 2. CRRES Frequency Ratios Versus L_T (Figure 7)

L_T	f_2/f_1	f_3/f_1
4–5	2.45 ± 0.32	3.83 ± 0.49
5–6	2.58 ± 0.24	4.07 ± 0.52
6–7	2.79 ± 0.31	4.26 ± 0.62
7–8	2.84 ± 0.27	4.27 ± 0.59

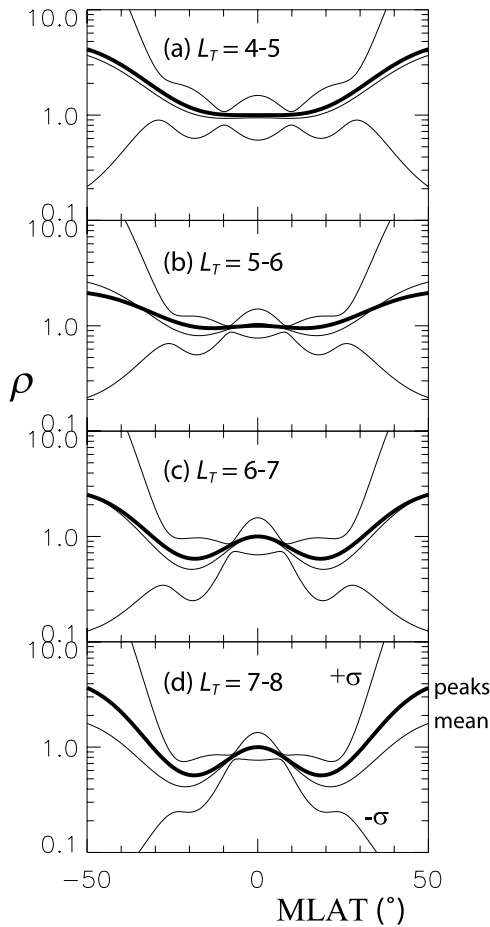


Figure 8. Inferred field line distributions of mass density ρ versus MLAT for (a) $L_T = 4-5$, (b) $L_T = 5-6$, (c) $L_T = 6-7$, and (d) $L_T = 7-8$. The bold curves are the polynomial solutions based on the peak frequencies in Table 2, whereas the thin curves are the log average solution (middle thin curve) and the log average plus or minus one standard deviation (upper and lower thin curves) based on a Monte Carlo simulation using a distribution of frequencies consistent with the standard deviations in the frequency ratios listed in Table 2.

polynomial solutions based on the peak frequency ratios in Table 2, whereas the thin curves are the log average solution (middle thin curve) and the log average plus or minus one standard deviation (upper and lower thin curves) based on a Monte Carlo simulation using a distribution of frequency ratios consistent with the standard deviations in the frequency ratios listed in Table 2 [Denton *et al.*, 2004a].

[28] The range of solutions between the upper and lower thin solid curves includes real variation in the field line distribution due to varying frequency ratios and is not just due to uncertainty in the measurements. Note that at low $L_T = 4-5$ (Figure 8a), the distribution based on the peak frequency ratios (thick solid curve) is fairly flat for $MLAT = -10$ to 10° and increases farther away from the magnetic equator. The results of the Monte Carlo simulation (thin solid curves) show that most of the Monte Carlo solutions are consistent with a monotonic dependence. (Note that at large $MLAT \gtrsim 30^\circ$, our solutions are very

uncertain. This results from the fact that the Alfvén frequencies are insensitive to the high-latitude part of the field line, where the magnetic field and the Alfvén speed are large.) However, at larger $L_T = 6-8$, the distribution based on the peak frequency ratios (thick solid curve) is locally peaked at the magnetic equator. (See the work of Takahashi *et al.* [2004] for an explanation of how particular values of the frequency ratio lead to the local peak in ρ .) The value of ρ at $MLAT = 0$ is about a factor of 2 larger than at the minimum, which occurs at about 20° . The results of the Monte Carlo simulation show that most solutions consistent with the range of frequency ratios in Table 2 are locally peaked (since the range of solutions within plus or minus one standard deviation at low MLAT is at higher density than the range of solutions within plus or minus one standard deviation at intermediate MLAT between about 10 and 25°). This is especially clear for $L_T = 7-8$ (Figure 8d).

[29] For the use of modelers, we now make some comparisons to solutions using the power law distribution (1). Figure 9 again shows the inferred field line distributions of mass density ρ versus MLAT, but this time, the polynomial solutions (thick solid curves) are plotted with solutions based on the power law form (1). All these solutions are found using the peak frequency ratios in Table 2. Again, only the relative variation in ρ is significant. However, the vertical variations between solutions in each panel is significant. The frequency is chosen such that the solution for $\alpha = 0$ has $\rho = 1$ amu. Figure 9 shows that larger positive values of α lead to smaller inferred equatorial mass density. At $L_T = 4-5$ (Figure 9a), ρ is fairly flat ($\alpha = 0$) within $MLAT = -10$ to 10° . However, considering the entire MLAT range plotted, the $\alpha = 2$ solution (thin dashed curve) does the best job of modeling the ρ dependence. At $L_T = 5-6$, $\alpha = 1$ appears to do the best job of modeling the entire MLAT range plotted. Note that Takahashi *et al.* [2004] suggested $\alpha = 0-1$ for modeling ρ at $L_T < 6$. For $L_T > 6$ (Figures 9c and 9d), there is a local peak in ρ at the magnetic equator. The power law distribution cannot accurately model the entire polynomial distribution, since it is not monotonic. The values of α implied by the frequency ratios are actually negative, since the low MLAT range has the largest effect on the frequencies. Over the entire MLAT range, however, the $\alpha = 1$ solution probably fits the polynomial solutions better than the others.

[30] Figure 10 is the same as Figure 9 except that the power law solutions (thin curves) are found using only the fundamental frequency. There is very little difference between the two figures, except that there is less variation in the solutions near to $MLAT = 0^\circ$. In Figure 10a ($L_T = 4-5$) the $\alpha = 1$ solution is now closer to the polynomial solution than the $\alpha = 2$ solution within $-20^\circ < MLAT < 20^\circ$. Nevertheless, at small MLAT, the difference between these solutions is small so that the $\alpha = 2$ solution is probably still a better choice considering the entire range of MLAT. For the other L_T ranges, $\alpha = 1$ leads to solutions that best match the polynomial form.

3.2. Field Line Distribution From Frequencies of Takahashi *et al.* [2004]: Other Factors

[31] In order to investigate what factors other than L_T might be influencing the local peak in ρ at $MLAT = 0$, we

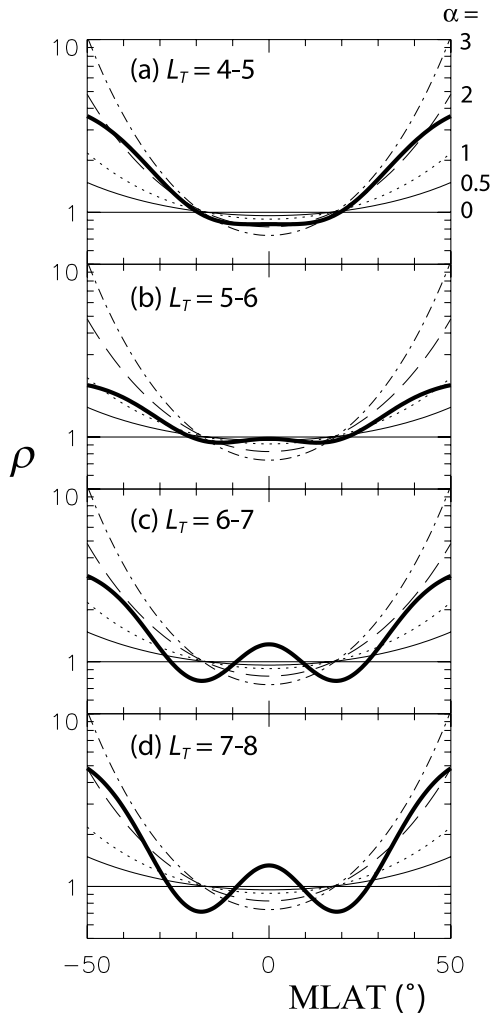


Figure 9. Inferred field line distributions of mass density ρ versus MLAT for (a) $L_T = 4-5$, (b) $L_T = 5-6$, (c) $L_T = 6-7$, and (d) $L_T = 7-8$. The bold curves are the polynomial solutions based on the peak frequencies in Table 2, whereas the thin curves are the power law solutions with $\alpha = 0$ (thin horizontal line at $\rho = 1$), 0.5 (thin solid curve), 1 (thin dotted curve), 2 (thin dashed curve), and 3 (thin dot dashed curve).

divide the data up into two groups based on the value of several parameters. For instance, Figure 11a shows the distribution of frequencies normalized to the fundamental frequency within $L_T = 4-6$ for two ranges of Dst, -33 to $+31$ (dashed curve) and -164 to -33 (solid curve). Figure 11a shows that the frequency ratios are not significantly correlated with Dst for $L_T = 4-6$ (because the dashed and solid curves are right on top of each other). Figure 11b shows the normalized frequencies within $L_T = 6-8$ for Dst = -31 to $+37$ (dashed curve) and -142 to -31 (solid curve). Figure 11b shows that the frequencies of the second and third harmonics are shifted to larger values relative to the fundamental at more negative values of Dst (solid curve) relative to the more positive values (dashed curve). At $L_T = 6-8$, we also found a similar shift of the frequency ratios to higher values as $\langle Kp \rangle_3$ and the wave energy (squared amplitude δE^2) were increased. Table 3 shows the values of f_2/f_1 and f_3/f_1 resulting from a two Gaussian fit for the

data within $L_T = 6-8$ in different ranges of $\langle Kp \rangle_3$, Dst, and δE^2 .

[32] Figure 12 shows the inferred field line distribution of ρ for the various combinations of f_2/f_1 and f_3/f_1 listed in Table 3. There is a larger local peak in ρ at MLAT = 0 for larger $\langle Kp \rangle_3$, more negative Dst, and larger wave amplitude δE^2 (right panels), relative to smaller values of $\langle Kp \rangle_3$, less negative Dst, and smaller δE^2 (left panels). The contrast is greatest for the wave amplitude, which may indicate that the ponderomotive force plays a role in driving heavy ions up the field line. The correlation with more negative Dst and larger $\langle Kp \rangle_3$ might be due to increasing dominance of the ring current. (More negative Dst correlates with increased ring current, and larger $\langle Kp \rangle_3$ correlates with less plasmaspheric density.)

[33] Some caution is in order in regard to these results. The peaks of f_n/f_1 in Table 3 have a large enough width so that the frequency ratios for different ranges of parameters overlap. For instance, f_2/f_1 is 2.70 ± 0.25 for $\delta E^2 = 10^{-6} - 0.0003$ (mV/m) 2 and 2.84 ± 0.33 for $\delta E^2 = 0.0003 - 0.1$ (mV/m) 2 , and if the widths are interpreted as uncertainties, 2.70 ± 0.25 is equal to 2.84 ± 0.33 within their uncertainties. However, the widths are not entirely due to uncertainty but

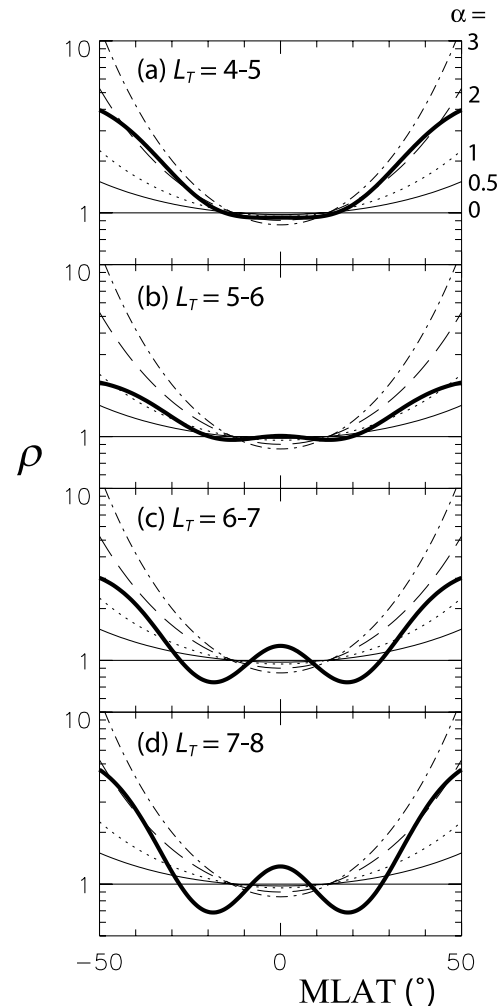


Figure 10. Same as Figure 9, except that the power law solutions are found using only the fundamental frequency.

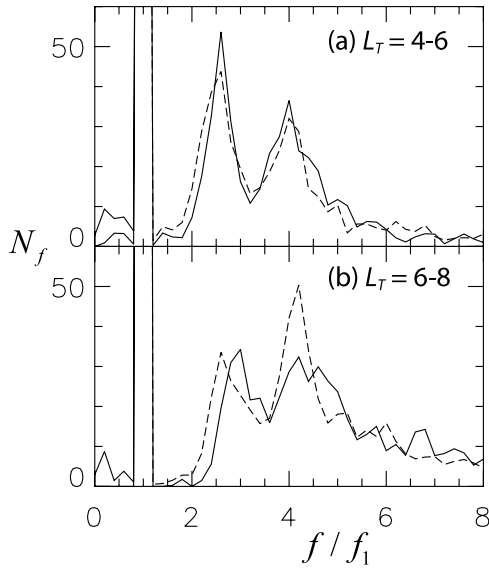


Figure 11. Distribution of the ratio of the toroidal Alfvén harmonic frequency f divided by the fundamental frequency f_1 for $L_T =$ (a) 4–6, and (b) 6–8. The dashed (solid) curve shows the distribution for the half of the data with the largest (most negative) Dst values. N_f is the number of wave observations in each bin of width 0.2.

also represent the real variation in the frequency ratios (at different times) for a certain parameter range. Nevertheless, there is some uncertainty, and it is probably of the order of the width, so these results must be regarded as somewhat tentative. For instance, considering the correlation with wave amplitude, it might be that the wave frequencies are better determined when the wave amplitude is large.

3.3. Summary of Inferred Distribution of Mass Density

[34] The results shown in section 3.1 support the conclusion of *Takahashi et al.* [2004] that there is a local peak in mass density at the magnetic equator for large L_T . *Takahashi et al.* [2004] were able to show this result for $L_T = 6-7$. The improvements in technique implemented here have allowed us to find average harmonic frequency ratios also for $L_T = 7-8$ and to demonstrate that the inferred mass density for this range of L_T is also locally peaked at the magnetic equator (Figure 8d). Peaking of the mass density at the magnetic equator could result from a potential well at the equator due to rotation. (The centrifugal force with constant frequency, as is appropriate for corotation, is proportional to the radius.) If the temperature of different ion species is roughly the same, then the potential well would proportionately have a greater effect on heavy ions (particularly O^+) and thus might lead to preferential concentration of heavy ions at the magnetic equator.

[35] We also examined the dependence of the average harmonic frequency ratios with respect to $\langle Kp \rangle_3$, Dst, and wave energy (δE^2) (section 3.2). At the lower values of L_T , there was no significant dependence of the frequency ratios on these quantities (for Dst, this is shown in Figure 11). However, at larger $L_T = 6-8$, there is greater peaking of the mass density for large $\langle Kp \rangle_3$, more negative Dst, and larger squared wave amplitude δE^2 (Figure 12). These results may

indicate the importance of the ponderomotive force and a ring current population of heavy ions.

[36] We also compared solutions of the field line distribution found using the power law field line distribution (1) with only the fundamental frequency as input, to the solutions using our polynomial distribution with all the frequencies (fundamental and second and third harmonics) as input (Figure 10). Here we found that the power law distribution with $\alpha = 1$ did a good job reproducing the result of the full solution (polynomial solution with all frequencies as input) for $L_T = 5-6$. At $L_T = 4-5$, the distribution based on the full solution was very flat within $|\text{MLAT}| \leq 20^\circ$ (implying a low value of $\alpha = 0-1$). However, considering the entire range of MLAT plotted in Figure 10, $\alpha = 2$ might be a better choice to describe the distribution. At larger $L_T > 6$, a monotonic field line distribution cannot well represent our results. However, if one chooses to use the power law form anyway, $\alpha = 1$ is probably the best choice.

4. Discussion

[37] A major goal of this paper was to examine the discrepancy between the inferred field line distribution of electron density from previous studies [*Goldstein et al.*, 2001; *Reinisch et al.*, 2001; *Denton et al.*, 2002a, 2002b, 2004b; *Reinisch et al.*, 2004; *Huang et al.*, 2004] and that of the mass density based on previous studies [*Denton et al.*, 2001, 2004a; *Takahashi et al.*, 2004]. In particular, no study of the field line distribution of electron density has yet found convincing evidence of a local peak in density at the magnetic equator, whereas the studies of the mass density based on field line resonance frequencies have found such a peak for $L_T > 6$. Our study is divided into two parts; section 2.4 summarizes our results for the field line distribution of electron density. As shown in section 2, the previous studies of the field line distribution of electron density were based on data sets that could not possibly reveal a local peak in density for $L_T > 6$. This is because the Polar data set [*Goldstein et al.*, 2001; *Denton et al.*, 2002a, 2002b, 2004b] did not sample low MLAT for $L_T > 6$ (Figures 3 and 4) and because studies of the field line distribution using IMAGE RPI have been at low L_T [*Reinisch et al.*, 2001, 2004; *Huang et al.*, 2004]. An inferred electron density distribution at $L_T = 7.4$ from IMAGE RPI data was presented in Figure 2, but again, low MLAT was not sampled. In order to see if there was any evidence for a peak in electron density at the magnetic equator, we examined CRRES data (Figures 5 and 6), but there appeared to be no convincing evidence for such a peak based on that data set.

[38] Section 3.3 summarizes our results for the field line distribution of mass density. The observed Alfvén frequen-

Table 3. CRRES Frequency Ratios at $L_T = 6-8$ Within a Parameter Range

Parameter Range	f_2/f_1	f_3/f_1
$\langle Kp \rangle_3 = 1.5 - 3.4$	2.75 ± 0.37	4.24 ± 0.47
$\langle Kp \rangle_3 = 3.4 - 5.9$	2.85 ± 0.27	4.27 ± 0.71
Dst = -31 - (+37)	2.72 ± 0.36	4.17 ± 0.41
Dst = -142 - (-31)	2.89 ± 0.26	4.40 ± 0.77
$\delta E^2 = 10^{-6} - 0.0003$ (mV/m) ²	2.70 ± 0.25	4.28 ± 0.60
$\delta E^2 = 0.0003 - 0.1$ (mV/m) ²	2.84 ± 0.33	4.24 ± 0.58

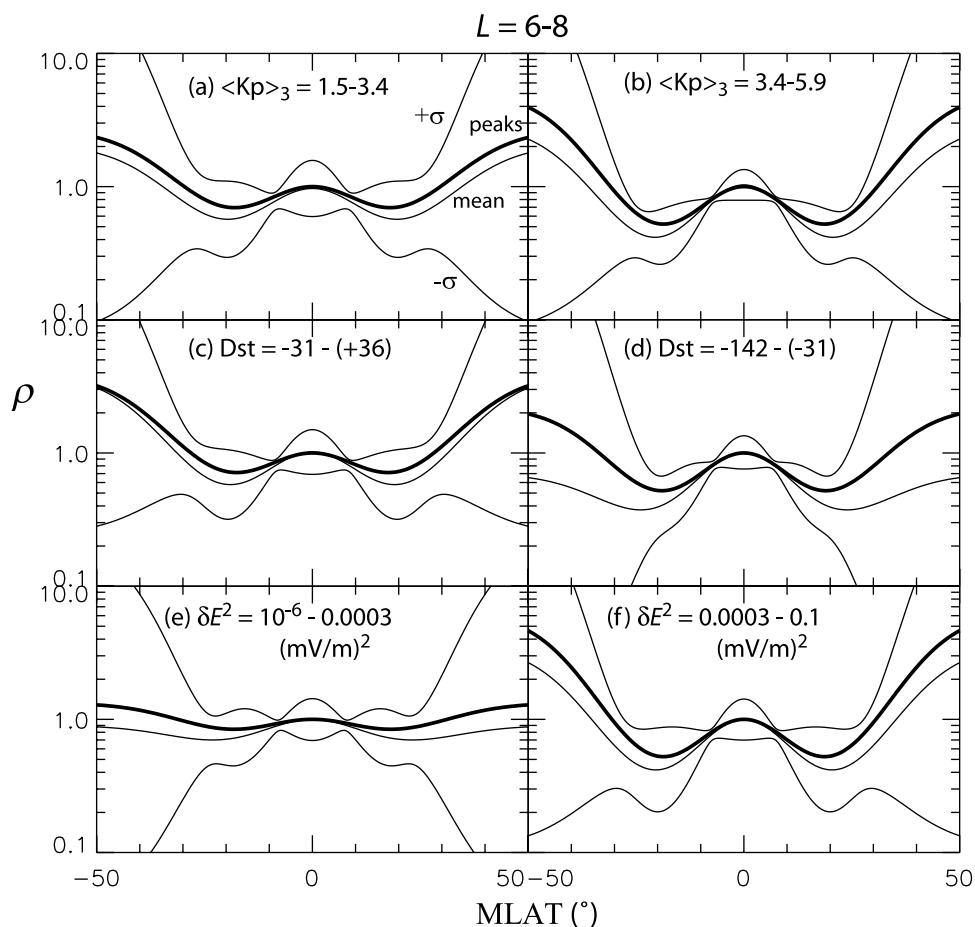


Figure 12. Inferred field line distributions of mass density ρ versus MLAT for $L_T = 6-8$ for (a) low $\langle Kp \rangle_3 < 3.4$, (b) high $\langle Kp \rangle_3 > 3.4$, (c) more positive Dst > -31 , (d) more negative Dst < -31 , (e) smaller wave amplitude $\delta E^2 < 0.0003 \text{ (mV/m)}^2$, and (f) larger wave amplitude $\delta E^2 > 0.0003 \text{ (mV/m)}^2$, based on the frequency ratios in Table 3. The curves in each panel have the same meanings as those in Figure 8.

cies imply that there is a local peak in mass density at the magnetic equator for $L_T = 6-8$, especially for large wave amplitude and large negative Dst. Taken together, the existence of a local peak in mass density while there is no such peak in electron density would seem to imply that heavy ions are on average preferentially concentrated at the magnetic equator. As we argued in the first paragraph of section 3.3, such preferential peaking could result from a potential well at the equator due to rotation. However, results in section 3.2 suggested that there is very little or no local peak in mass density even at $L_T = 6-8$ if we confine the data to low Alfvén wave amplitude ($\delta E^2 < 0.0003 \text{ (mV/m)}^2$). Our average inferred distributions of electron density (Figures 5 and 6) were found at all times, not just those times when Alfvén wave harmonics were observed. In order to investigate whether the electron density might be locally peaked at the magnetic equator during times for which strong Alfvén waves are observed, we recalculated the log average electron density versus MLAT for the CRRES data in the range $L_T = 6-7$, but now limiting the data to times during which Alfvén wave harmonics are observed with $\delta E^2 > 0.0003 \text{ (mV/m)}^2$. The results are shown in Figures 13b and 13d. For comparison, Figures 13a and 13c shows the results using all the data (same as Figures 5g and 5j). It is clear that this data also

does not give any evidence for a local peak in electron density.

[39] One further caution about the mass density inferred from Alfvén wave frequencies relates to our assumption of a

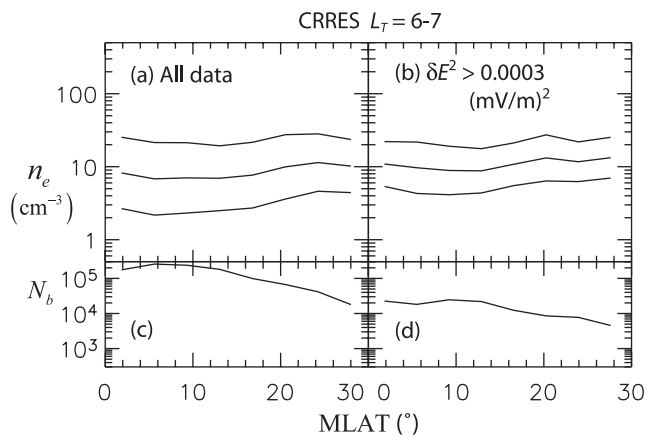


Figure 13. (a) and (c) Identical to Figures 5g and 5j. (b) and (d) The same, except the data has been limited to times during which Alfvén wave harmonics are observed with $\delta E^2 > 0.0003 \text{ (mV/m)}^2$.

perfectly conducting ionosphere. We have not yet conducted successful mass density inversions with finite resistivity at the ionospheric boundaries. In order to see if the apparent peak in mass density at the equator could be related to a faulty boundary condition (which could lead to different wavelengths and frequency ratios, and different symmetry for the solutions), we calculated the average frequency ratios again for $L_T = 6-8$, but this time limiting the observed wave frequencies to those cases for which $MLT = 8-16$ (dayside). In this range of MLT, we expect the ionospheric foot points of the field lines to be lit by the Sun so that the ionospheric conductivity is high. For this data, we find that $f_2/f_1 = 2.81 \pm 0.29$ and $f_3/f_1 = 4.24 \pm 0.60$. These ratios are similar to those listed in Table 2 for $L_T = 6-7$ and $7-8$, including all MLT values. Therefore the inferred peak in local mass density is probably not due to an incorrect assumption about the ionospheric conductivity.

[40] Our data suggests, then, that heavy ions are preferentially concentrated at the magnetic equator for $L_T > 6$, at least during active times with wave activity. We have also included results useful for modelers. If one uses the power law distribution (1) to model the field line distribution of mass density, $\alpha = 1$ is the best choice for $L_T > 5$, while $\alpha = 2$ may be better for $L_T = 4-5$.

[41] **Acknowledgments.** We thank Bill Lotko for useful conversations. We are grateful to Iowa PWI team, including J. D. Menietti, D. Gurnett, and J. Pickett, for supplying the upper hybrid resonance data (supported by NASA grant NAG5-11942), the Polar spacecraft science data team for supplying spacecraft ephemeris data, and NSSDC for making the IMP-8 (GSFC and LANL) and WIND (courtesy of R. P. Lepping and K. W. Ogilvie) solar wind data, Dst (Kyoto University), and Kp (NOAA) data available on OMNIWeb. Work at Dartmouth and APL was supported by NASA grant NAG5-12201. Work at Dartmouth was further supported by NASA grant NAG5-11825 and by NSF grant ATM-0245664.

[42] Arthur Richmond thanks Frederick Menk and Peter Chi for their assistance in evaluating this paper.

References

- Denton, R. E., E. G. Miftakhova, M. R. Lessard, R. Anderson, and J. W. Hughes (2001), Determining the mass density along magnetic field lines from toroidal eigenfrequencies: Polynomial expansion applied to CRRES data, *J. Geophys. Res.*, *106*, 29,915.
- Denton, R. E., J. Goldstein, J. D. Menietti, and S. L. Young (2002a), Magnetospheric electron density model inferred from Polar plasma wave data, *J. Geophys. Res.*, *107*(A11), 1386, doi:10.1029/2001JA009136.
- Denton, R. E., J. Goldstein, and J. D. Menietti (2002b), Field line dependence of magnetospheric electron density, *Geophys. Res. Lett.*, *29*(24), 2205, doi:10.1029/2002GL015963.
- Denton, R. E., K. Takahashi, R. R. Anderson, and M. P. Wuest (2004a), Magnetospheric toroidal Alfvén wave harmonics and the field line distribution of mass density, *J. Geophys. Res.*, *109*, A06202, doi:10.1029/2003JA010201.
- Denton, R. E., J. D. Menietti, J. Goldstein, S. L. Young, and R. R. Anderson (2004b), Electron density in the magnetosphere, *J. Geophys. Res.*, *109*, A09215, doi:10.1029/2003JA010245.
- Denton, R. E., et al. (2006), Realistic magnetospheric mass density model for 29 August 2000, *J. Sol. Terr. Phys.*, *68*, 625.
- Elkington, S. R., M. K. Hudson, and A. A. Chan (2003), Resonant acceleration and diffusion of outer zone electrons in an asymmetric geomagnetic field, *J. Geophys. Res.*, *108*(A3), 1116, doi:10.1029/2001JA009202.
- Gallagher, D. L., P. D. Craven, and R. H. Comfort (1988), An empirical model of the Earth's plasmasphere, *Adv. Space Res.*, *8*, 15.
- Gallagher, D. L., P. D. Craven, and R. H. Comfort (2000), Global core plasma model, *J. Geophys. Res.*, *105*, 18,819.
- Goldstein, J., R. E. Denton, M. K. Hudson, E. G. Miftakhova, S. L. Young, J. D. Menietti, and D. L. Gallagher (2001), Latitudinal density dependence of magnetic field lines inferred from Polar plasma wave data, *J. Geophys. Res.*, *106*, 6195.
- Huang, X., B. W. Reinisch, P. Song, J. L. Green, and D. L. Gallagher (2004), Developing an empirical density model of the plasmasphere using IMAGE/RPI observations, *Adv. Space Res.*, *33*, 829.
- LeDocq, M. J., D. A. Gurnett, and R. R. Anderson (1994), Electron number density fluctuations near the plasmopause observed by the CRRES spacecraft, *J. Geophys. Res.*, *99*, 23,661–23,671.
- Lemaire, J. F., and K. I. Gringauz (1998), *The Earth's Plasmasphere*, pp. 222–249, Cambridge Univ. Press, New York.
- Meredith, N. P., R. M. Thorne, R. B. Horne, D. Summers, B. J. Fraser, and R. R. Anderson (2003), Statistical analysis of relativistic electron energies for cyclotron resonance with EMIC waves observed on CRRES, *J. Geophys. Res.*, *108*(A6), 1250, doi:10.1029/2002JA009700.
- Nsumei, P. A., X. Huang, B. W. Reinisch, P. Song, V. M. Vasyliunas, J. L. Green, S. F. Fung, R. F. Benson, and D. L. Gallagher (2003), Electron density distribution over the northern polar region deduced from IMAGE/radio plasma imager sounding, *J. Geophys. Res.*, *108*(A2), 1078, doi:10.1029/2002JA009616.
- Perry, K. L., M. K. Hudson, and S. R. Elkington (2005), Incorporating spectral characteristics of Pc5 waves into three-dimensional radiation belt modeling and the diffusion of relativistic electrons, *J. Geophys. Res.*, *110*, A03215, doi:10.1029/2004JA010760.
- Reinisch, B. W., X. Huang, P. Song, G. S. Sales, S. F. Fung, J. L. Green, D. L. Gallagher, and V. M. Vasyliunas (2001), Plasma density distribution along the magnetospheric field: RPI observations from IMAGE, *Geophys. Res. Lett.*, *28*, 4521.
- Reinisch, B. W., X. Huang, P. Song, J. L. Green, S. F. Fung, V. M. Vasyliunas, D. L. Gallagher, and B. R. Sandel (2004), Plasmaspheric mass loss and refilling as a result of a magnetic storm, *J. Geophys. Res.*, *109*, A01202, doi:10.1029/2003JA009948.
- Sheeley, B. W., M. B. Moldwin, and H. K. Rassoul (2001), An empirical plasmasphere and trough density model: CRRES observations, *J. Geophys. Res.*, *106*, 25,631.
- Singer, H. J., D. J. Southwood, R. J. Walker, and M. G. Kivelson (1981), Alfvén wave resonances in a realistic magnetospheric magnetic field geometry, *J. Geophys. Res.*, *86*, 4589.
- Spasojevic, M., H. U. Frey, M. F. Thomsen, S. A. Fuselier, S. P. Gary, B. R. Sandel, and U. S. Inan (2004), The link between a detached subauroral proton arc and a plasmaspheric plume, *Geophys. Res. Lett.*, *31*, L04803, doi:10.1029/2003GL018389.
- Summers, D., C. Ma, and T. Mukai (2004), Competition between acceleration and loss mechanisms of relativistic electrons during geomagnetic storms, *J. Geophys. Res.*, *109*, A04221, doi:10.1029/2004JA010437.
- Takahashi, K., R. E. Denton, R. R. Anderson, and W. J. Hughes (2004), Frequencies of standing Alfvén wave harmonics and their implication for plasma mass distribution along geomagnetic field lines: Statistical analysis of CRRES data, *J. Geophys. Res.*, *109*, A08202, doi:10.1029/2003JA010345.
- Tsyganenko, N. A. (1989), A magnetospheric magnetic field model with a warped tail current sheet, *Planet. Space Sci.*, *37*, 5.
- Tsyganenko, N. A. (1995), Modeling the Earth's magnetospheric magnetic field confined within a realistic magnetopause, *J. Geophys. Res.*, *100*, 5599.
- R. R. Anderson, Department of Physics and Astronomy, University of Iowa, Iowa City, IA 52242, USA. (jdm@space.physics.uiowa.edu)
- R. E. Denton and M. K. Sleeper, Department of Physics and Astronomy, Dartmouth College, 6127 Wilder Laboratory, Hanover, NH 03755, USA. (redenton@dartmouth.edu)
- I. A. Galkin, X. Huang, P. Nsumei, and B. W. Reinisch, Center for Atmospheric Research, University of Massachusetts at Lowell, 600 Suffolk Street, Lowell, MA 01854, USA. (paul_song@uml.edu)
- W. J. Hughes, Department of Astronomy, Boston University, Boston, MA 02215, USA. (hughes@bu.edu)
- K. Takahashi, Johns Hopkins University Applied Physics Laboratory, 11100 Johns Hopkins Road, Laurel, MD 20723, USA. (kazue.takahashi@jhuapl.edu)